

ACAGTTTGTG-3'; (ii) 5'-CCCATCGATTTAACTCC-TCAAGTGAATGAG-3'. XIAP_{H467A} and c-IAP1_{H588A} were made by using the QuikChange site-directed mutagenesis kit (Stratagene, La Jolla, CA) with primers (i) 5'-GTTTTTGTTCCTGTGGAGCTAGTCAC-TTGTAACAA-3' and 5'-TTGTTTACAAGTGACTA-GAGCTCCACAAGGAACAAAAC-3'; (ii) 5'-CTGT-TGTATTTATTCCTGTGGTCTGGTAGTATGCCA-GGAATGTGC 3' and 5' GCACATTCCTGGCATACTACCAGAGCACCACAAGGAATAACAACAG-3'. These cDNAs were cloned into pGEX-4T-2 by using Bam HI and Not 1 sites and confirmed by direct sequencing. The GST or GST fusion proteins were induced in DH-5 α cells with 200 μ M IPTG (isopropyl- β -D-thiogalactopyranoside) and purified with glutathione-Sepharose 4B. In vitro ubiquitination reactions were carried out by adding recombinant wheat

E1 (20 ng), UbcH5b (20 ng), 2 μ l of bacterial lysate from BL-21 cells, and ³²P-labeled ubiquitin (2×10^4 cpm) to the GST or GST fusion proteins in ubiquitination buffer [50 mM Tris (pH 7.4), 2 mM adenosine 5'-triphosphate, 5 mM MgCl₂, and 2 mM dithiothreitol]. After incubating at 30°C for 90 min, the reaction mixtures were separated by 7.5% SDS-PAGE and visualized with a Storm PhosphorImager and ImageQuant software (Molecular Dynamics). After exposure, the gels were restained with Coomassie blue to ensure that similar amounts of the GST fusion proteins had been used.

12. 2B4.11 T hybridoma cells were transfected with pEBB-Flag-XIAP, pEBB-Flag-XIAP_{H467A}, or pEBB-Flag-XIAP₁₋₃₅₁ together with pCI-neo. The cells were selected with G418 (1 mg/ml) and screened with anti-Flag for expression of the transfected

molecules. Two independent cell lines expressing XIAP (XFL1 and XFL2) and one cell line expressing XIAP₁₋₃₅₁ (XT) were found to have similar levels of the transfected molecules and were used for further study.

13. R. Takahashi et al., *J. Biol. Chem.* **273**, 7787 (1998)
14. R. J. Clem and L. K. Miller, *Mol. Cell. Biol.* **14**, 5212 (1994); D. Vucic, W. J. Kaiser, L. K. Miller, *J. Biol. Chem.* **273**, 33915 (1998); B. A. Hay, D. A. Wasserman, G. M. Rubin, *Cell* **83**, 1253 (1995).
15. L. J. Eiben and C. S. Duckett, *Results Probl. Cell Differ.* **24**, 91 (1998).
16. We are grateful to C. Duckett (National Cancer Institute, Bethesda, MD) for providing human XIAP and c-IAP1 cDNAs and for critical review of this manuscript.

10 January 2000; accepted 20 March 2000

Seeing the Herpesvirus Capsid at 8.5 Å

Z. Hong Zhou,¹ Matthew Dougherty,² Joanita Jakana,² Jing He,³ Frazer J. Rixon,⁴ Wah Chiu^{2,3*}

Human herpesviruses are large and structurally complex viruses that cause a variety of diseases. The three-dimensional structure of the herpesvirus capsid has been determined at 8.5 angstrom resolution by electron cryomicroscopy. More than 30 putative α helices were identified in the four proteins that make up the 0.2 billion-dalton shell. Some of these helices are located at domains that undergo conformational changes during capsid assembly and DNA packaging. The unique spatial arrangement of the heterotrimer at the local threefold positions accounts for the asymmetric interactions with adjacent capsid components and the unusual co-dependent folding of its subunits.

Human herpesviruses cause a variety of disorders ranging from cold sores and chicken pox to less frequent conditions, including congenital defects, blindness, and cancers as well as life-threatening complications in immunosuppressed individuals (1, 2). Herpes simplex virus-type 1 (HSV-1), the prototypical member of the herpesvirus family, infects more than 60% of the United States population. The HSV-1 genome of 150,000 base pairs (bp) contains over 75 open reading frames, about half of which encode structural proteins. The herpesvirus virion is composed of a glycoprotein-containing envelope, a proteinaceous layer (tegument), and an icosahedral capsid shell of 1250 Å diameter enclosing a double-stranded DNA (dsDNA) genome (3). Upon entry to the cell, the external compartments disassemble, releasing the capsid, which is transported across the cytosol in

association with cellular carrier proteins (4). At the nuclear pore, the viral DNA is released into the nucleus (5). New capsids are assembled around a scaffolding core inside the nucleus. Subsequently, viral DNA is packaged, possibly through a penton channel, after proteolysis and removal of scaffolding proteins (6).

We imaged ice-embedded HSV-1 capsids in a JEOL 4000 electron cryomicroscope with a LaB₆ gun operated at 400 kV (7). Despite their low contrast (Fig. 1A), the images contain data extending beyond 7 Å (Fig. 1B). By merging 5860 particle images from 130 micrographs (8), we determined the molecular structure to 8.5 Å resolution (Fig. 1, C through F). The validity of our structure can be gauged from several lines of evidence. These include the low-phase residuals (<45° at 8.5 Å) between two independent three-dimensional (3D) reconstructions (Fig. 1D) and the low (~58°) average-phase residual difference between raw images and computed projections from the final map up to 8.5 Å. The high degree of sixfold symmetry evident around the regions of the local sixfold symmetry axes was not enforced in the icosahedral reconstruction (Fig. 1E) and further supports the validity of the structure.

The capsid shell, with a total molecular mass of 0.2 billion daltons, is formed by four

proteins whose sequences are unrelated: VP5 (149 kD), VP26 (12 kD), VP23 (34 kD), and VP19C (50 kD). An asymmetric unit has a molecular mass of ~3.2 MD and consists of 1 penton subunit, 15 hexon subunits, and 5½ triplexes (Fig. 1F). The major morphological units in the capsid are the pentons and the hexons, which contain five and six copies of VP5, respectively. The hexon also contains six copies of VP26, which form a ring of connected densities on top of the VP5 subunits (9).

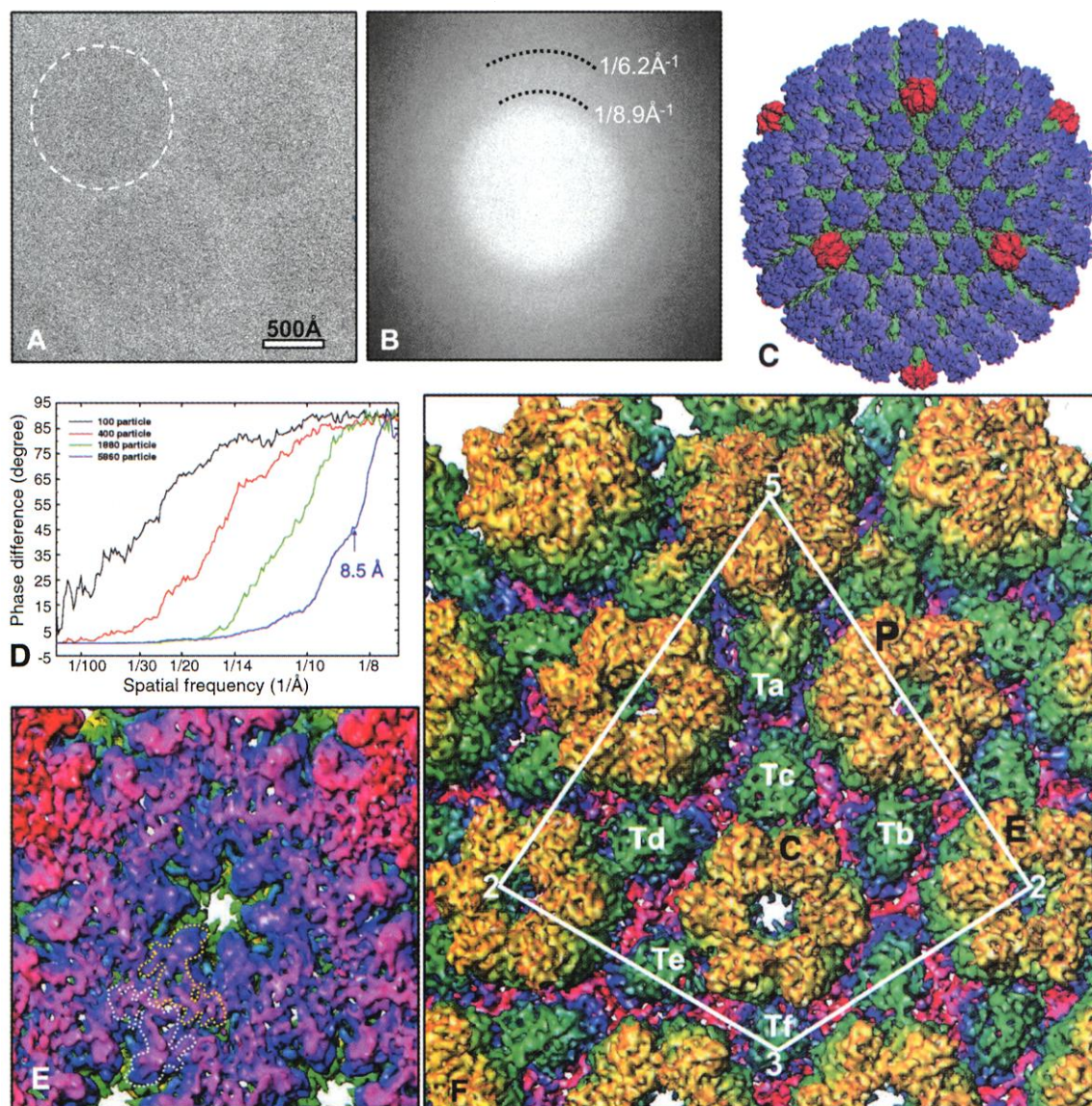
Previous studies of smaller viral capsids have demonstrated that α helices can be identified at 7.4 to 9 Å resolution (10–12). At this resolution range, the mass densities of α helices have the appearance of continuous high-density rods of 5 to 7 Å diameter. We have designated a relatively high density as an α helix when it forms an extended rod of the correct diameter and is spatially resolved from neighboring densities.

In the VP5 subunit of a sixfold averaged hexon (Fig. 2A), we assigned 24 mass segments as α helices (Fig. 2B). The VP26 subunit of the hexon contains no obvious candidate helices, in agreement with its reported secondary structure (13). On the basis of estimates of the number of amino acids involved, the putative α helices represent ~17% of the total mass of VP5, which is of the same range as the helical content of purified VP5 estimated by far ultraviolet (UV) circular dichroism (CD) spectroscopy (14). Two relatively long helices (20 and 22 Å) are present in the upper domain of the VP5 subunit (Fig. 2B). A group of seven relatively short (8 to 14 Å), nearly parallel α helices is seen in the middle domain (Fig. 2, B and C). These helices are close to the narrowest constriction of the channel that runs through the center of the hexons and pentons (Fig. 1C). In pentons, this channel appears to play an important role in capsid maturation and DNA packaging (6). It is closed in virions, presumably to prevent the exit of the packaged DNA, but is open in purified capsids that lack DNA (15). The closure of the channel occurs in the region of the constriction and requires a mass

¹Department of Pathology and Laboratory Medicine, University of Texas–Houston Medical School, Houston, TX 77030, USA. ²National Center for Macromolecular Imaging, Department of Biochemistry and Molecular Biology, Baylor College of Medicine, Houston, TX 77030, USA. ³Graduate Program in Structural and Computational Biology and Molecular Biophysics, Baylor College of Medicine, Houston, TX 77030, USA. ⁴MRC Virology Unit, Institute of Virology, Glasgow G11 5JR, Scotland, UK.

*To whom correspondence should be addressed. E-mail: wah@bcm.tmc.edu

Fig. 1. Electron cryomicroscopy and 3D reconstruction of HSV-1 B-capsids. **(A)** An area of a typical 400-kV image of ice-embedded capsids recorded in JEOL 4000 electron cryomicroscope at 50,000 \times magnification under a dose of \sim 12 electrons/ \AA^2 (7, 28). The defocus in the whole data set ranges from 0.2 to 1.8 μm . **(B)** An incoherent average of the Fourier transforms of 50 boxed-out particle images (29). Dashed arcs indicate the first and second zeros of the contrast transfer function at 1/8.9 and 1/6.2 \AA^{-1} , respectively. **(C)** Shaded surface view of the triangulation number $T = 16$ HSV-1 capsid with 12 pentons (red), 150 hexons (blue), and 320 triplexes (green). **(D)** Phase residual difference between two independent reconstructions as a function of resolution for data sets of different numbers of particles. The effective resolution of the reconstruction is based on the 45° phase residual difference, which is consistently improved as the number of particle images used for reconstruction increases. **(E)** A radially color-coded surface representation of the inner capsid surface of the 8.5 \AA reconstruction in the region surrounding a C hexon that is shown in **(F)**. This reveals the excellent sixfold symmetry in the floor domains of VP5, two of which are denoted by dotted lines. **(F)** A radially color-coded surface representation of the outer capsid surface of the 8.5 \AA reconstruction. An asymmetric unit, defined by the icosahedral five-, three-, and twofold axes (indicated by the labels 5, 3, and



2), is enclosed by the white line. A penton (labeled 5), the three types of hexon (designated P, E, and C), and the six types of triplex (labeled T_a , T_b , T_c , T_d , T_e , and T_f) are shown. The maps are displayed at a contour level of 1σ (standard deviation). All displays were generated with Iris Explorer (NAG, Downers Grove, Illinois) with custom-designed modules.

translocation in VP5, which probably involves sequences present in some of the adjacent helices. In the floor domain, a long (\sim 22 \AA) helix is joined through a slight bend to another long helix (\sim 26 \AA), which extends into the floor domain of the neighboring subunit (Fig. 2D). Previously, we have localized the region of contact between the scaffolding protein and the capsid shell to the region of the floor domain occupied by the distal end of this extended helix (16). It has recently been established that the NH_2 -terminus of VP5 is involved in the interaction with the scaffolding protein (17). Thus, it seems likely that this long helix may lie near the NH_2 -terminus of VP5. The insertion of the terminal helical fragment into the adjacent subunit may be a

mechanism for maintaining capsid stability, as has been shown in other animal viruses (18, 19). Several other helices can be identified in the floor domain (Fig. 2B), including one helix (\sim 14 \AA) that lies approximately parallel with and five helices (\sim 10 to 16 \AA) that lie perpendicular to the inner surface of the capsid (Fig. 2, B and D). Because the gross organization of the VP5 domains that constitute the floor domain changes markedly during capsid maturation (20), the existence and spatial arrangement of these helices will be influenced by the state of capsid morphogenesis.

Triplexes are characteristic features of herpesvirus capsids that link adjacent capsomeres. In HSV-1 the triplex was believed to be a

heterotrimer of one VP19C and two VP23 molecules (21, 22). However, it was not obvious how such a heterotrimer could be arranged around a quasi-threefold symmetrical position. To enhance the contrast of their structural features, we computationally aligned and averaged four of the triplexes occupying the local threefold positions surrounding the C hexon (Fig. 1F), together with their associated floor densities. We segmented the triplex graphically to delineate the approximate molecular boundaries of its protein components (Fig. 3, A to D). These assignments, which take the known molecular masses into account, were based on the continuity of mass densities and on the assumption of structural similarity between the two VP23 molecules and dissimilarity between the

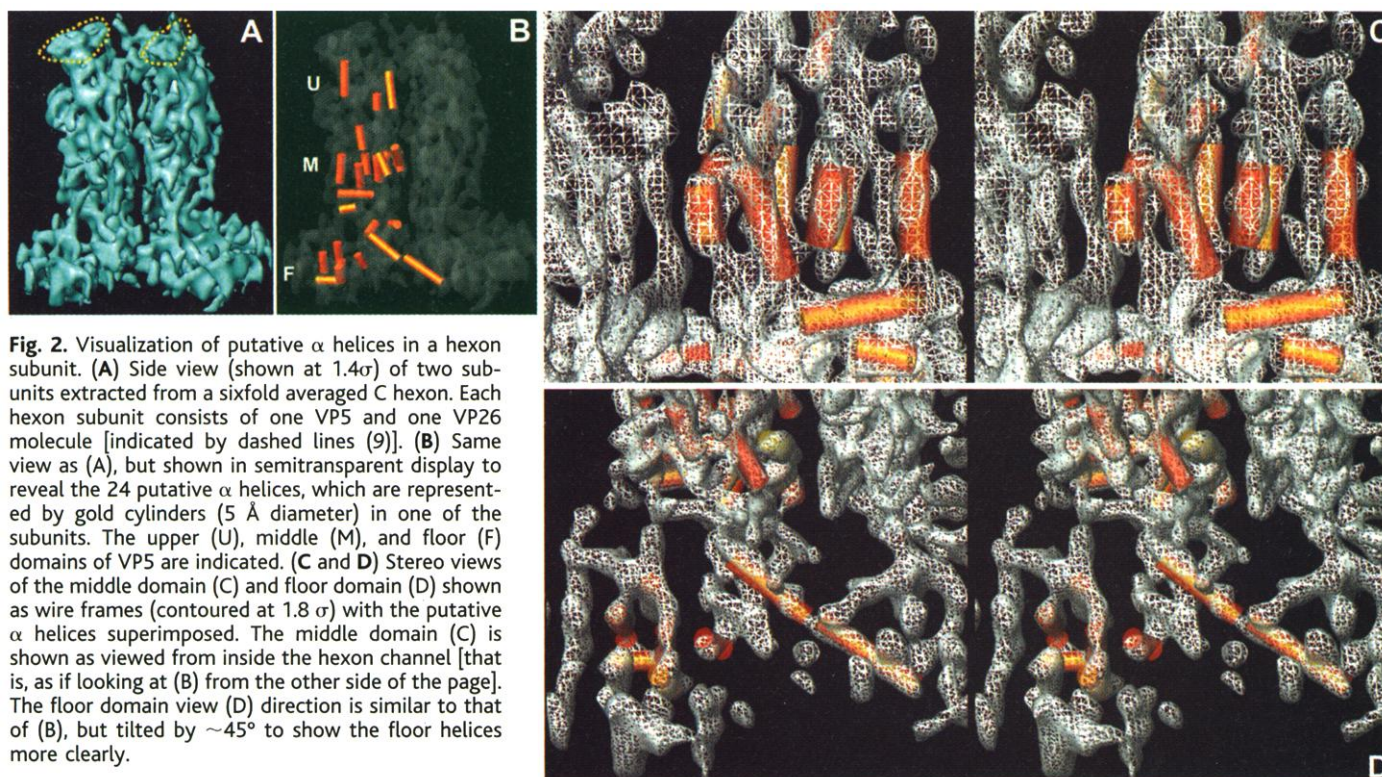


Fig. 2. Visualization of putative α helices in a hexon subunit. (A) Side view (shown at 1.4σ) of two subunits extracted from a sixfold averaged C hexon. Each hexon subunit consists of one VP5 and one VP26 molecule [indicated by dashed lines (9)]. (B) Same view as (A), but shown in semitransparent display to reveal the 24 putative α helices, which are represented by gold cylinders (5 Å diameter) in one of the subunits. The upper (U), middle (M), and floor (F) domains of VP5 are indicated. (C and D) Stereo views of the middle domain (C) and floor domain (D) shown as wire frames (contoured at 1.8σ) with the putative α helices superimposed. The middle domain (C) is shown as viewed from inside the hexon channel [that is, as if looking at (B) from the other side of the page]. The floor domain view (D) direction is similar to that of (B), but tilted by $\sim 45^\circ$ to show the floor helices more clearly.

VP23 and VP19C components. The overall relative dispositions of the VP23 and VP19C observed here are consistent with those suggested by the difference map between the inter-hexon connections in recombinant VP5-19C particles and intact capsids (23).

The floor density beneath the triplex (Fig. 3E) exhibits excellent threefold symmetry, reflecting the origin of this region, which is formed primarily by domains of VP5 from the three surrounding hexons. The densities in the lower third of the triplex are also triangularly related because the two VP23 and one VP19C occupy threefold equivalent positions (Fig. 3F). In this region, therefore, the triplex has the form of a pseudotrimer with each of the three triplex proteins, interacting, in a roughly similar manner, with each other and with the floor (VP5) densities from two hexon subunits (Fig. 3, A to C, E, and F). This triangular arrangement has altered by the middle region of the triplex (Fig. 3G), where the relative angular relation of the two VP23 molecules has changed to a more typical 180° dimeric configuration that no longer has an equivalent relation with VP19C. The upper part of the triplex (Fig. 3H) shows no evidence of structurally related features, and the bulk of this density is contributed by VP19C (23). The pattern of interactions revealed by these analyses illustrates the unusual nature of this complex. The two VP23 molecules interact with each other and with VP19C in very different ways. For example, at the lower part of the triplex, one side of one VP23 (gray color) forms the dimer interface

between the two VP23 molecules, whereas the equivalent side of the other VP23 (white color) forms an extensive interface with VP19C (Fig. 3, A to C and F). This is possible because particular regions of the proteins can participate in more than one type of interaction.

By examining the triplex density map for α helical content with the same criteria we used for VP5, we identified five short α helices (5 to 8 Å) in VP19C (24), whereas each VP23 contains three long (19 to 26 Å) α helices (Fig. 3I). We aligned the two VP23 subunits in a similar orientation to demonstrate the extent of their structural variation (Fig. 3J). Both the gross features and the three long helices are well conserved between the two molecules. However, large domain movements are evident between the dimer subunits. For example, the upper helix in each VP23 (denoted by asterisk in Fig. 3J) is oriented differently relative to the bulk of the molecule. It is probable that the different conformations of the two VP23 molecules within a triplex, which account for the alteration in their relation (Fig. 3, F and G), are needed to accommodate the sterically diverse interactions described here. Conformational adaptability is a recurring theme among viral capsid proteins as seen, for example, in the dimeric inner shell protein of bluetongue virus (19). This requirement for adaptability in VP23 may account for the observation that VP23 exists as a molten globule in isolation (25) but adopts a defined tertiary structure in the presence of VP19C. Furthermore, the contacts between VP23 and VP5 in the floor

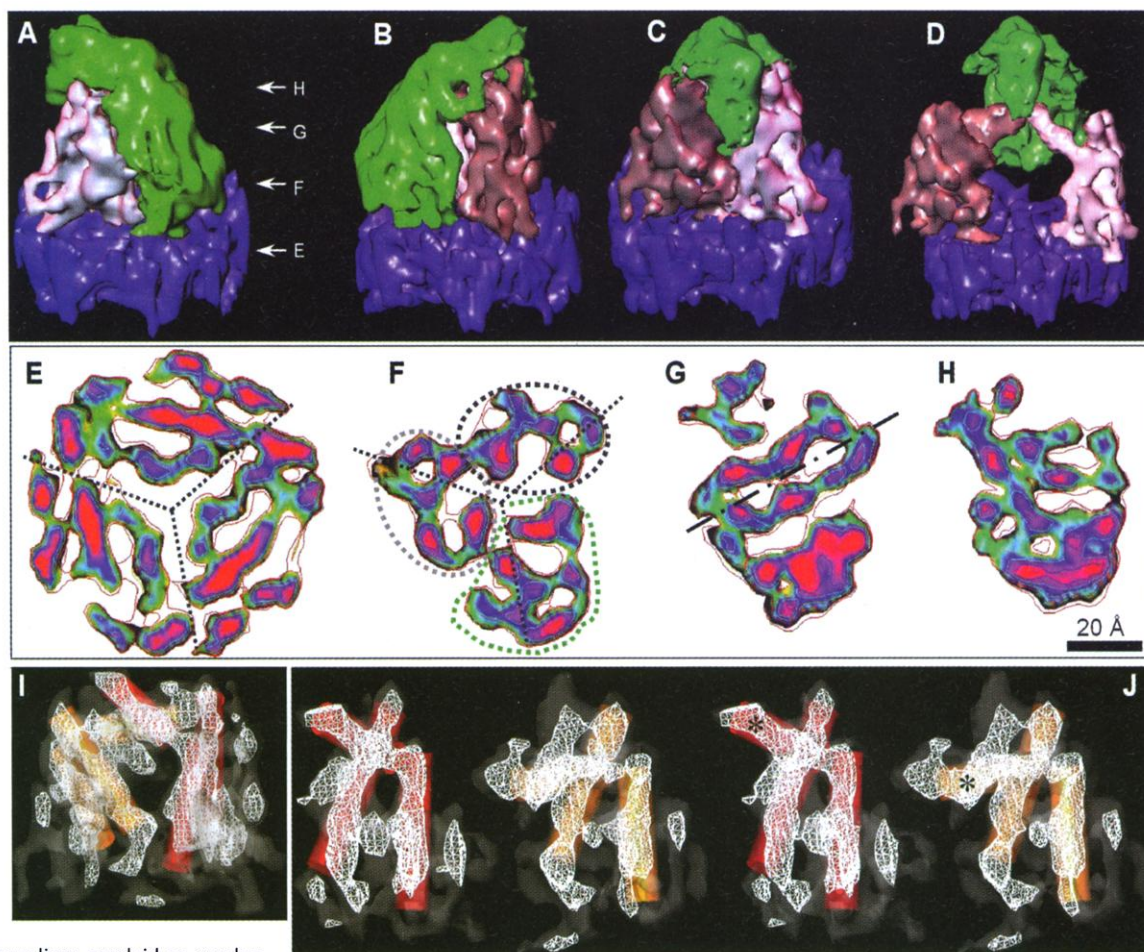
domain can only be formed as a late event in capsid assembly because their floor densities were not seen in the reconstruction map of the capsid progenitor, the procapsid (20). Therefore, the triplex represents a previously unknown type of protein complex, with a unique quaternary structure arrangement resulting from an unusual codependent folding of its subunits.

Our results have revealed some of the secondary structural elements in the proteins of the HSV capsid shell. In the viral structural proteins studied to date, relatively few types of protein fold have been identified, the most common of which is the β sandwich (26). By contrast, the recently elucidated structures of the core of the bluetongue virus (19) and the hepatitis B virus (10, 11, 27) show predominately α helices. Although our structure cannot yet describe the folds of individual proteins, the distributions of the α helices seen in VP5 and VP23 do not resemble those found in any known viral structures. Because VP5 is such a large molecule, it is likely to consist of multiple domains, each of which may have distinct folds.

References and Notes

1. B. N. Fields et al., Eds., *Fields Virology* (Lippincott-Raven, Philadelphia, 1996), vol. 2.
2. B. N. Roizman and A. E. Sears, in (1), pp. 2231–2295; R. J. Whitley, in (1), pp. 2297–2342; W. J. Britt and C. A. Alford, in (1), pp. 2493–2524; A. M. Arvin, in (1), pp. 2547–2586; A. B. Rickinson and E. Kieff, in (1), pp. 2397–2446; T. F. Schulz, Y. Chang, P. S. Moore, in *Human Tumor Viruses*, D. J. McCance, Ed. (American Society for Microbiology Press, Washington, DC, 1998), pp. 87–134.
3. A. C. Steven and P. G. Spear, in *Structural Biology of*

Fig. 3. Visualization of heterotrimeric interactions in the triplex. (A to C) Three side views (each rotated by 120° around the local threefold axis and displayed at slightly tilted angles) of the triplex obtained by averaging the four triplexes (T_b , T_c , T_d , T_e , as labeled in Fig. 1F) around the C hexon. Different colors are used to delineate VP19C (green), the two VP23 molecules (white and gray), and the floor (blue), which is formed by domains of VP5. (D) Same view as (C) but the VP19C and VP23 molecules are separated to reveal their organization. The shaded surface displays in (A) to (D) are contoured at 1.1 σ . (E to H) Representative 1.4-Å thick horizontal (that is, normal to the local threefold axis) slices through the averaged triplex at the positions indicated by arrows in (A). Each slice is shown with thin contour lines overlaid on a color display that gradates from red, through purple, to green, representing high-, median-, and low-density levels, respectively. The slice through the floor (E) exhibits excellent threefold symmetry and shows three density regions related by 120° rotations as indicated by the dotted lines. In (F), two similar density regions corresponding to the two VP23 molecules (indicated by light and dark ellipses) can be recognized, which are also related by a 120° rotation. The third density region (indicated by green dotted line) corresponds to VP19C. In (G), the two VP23 molecules (appearing as a flattened ring) are related by an ~180° rotation, as indicated by the dashed line, with VP19C present on either side. The top slice (H), which passes predominantly through VP19C densities, has an entirely asymmetric appearance. (I and J) identi-



fication of putative α helices in VP23. The maps are shown with wire frame displays (contoured at 1.5 σ), superimposed on gray semitransparent surface views contoured at a lower density level (1.1 σ). The putative α helices in the two VP23 molecules are depicted as red and gold cylinders of 5 Å diameter, respectively. The view direction of (I) is the same as in (C) but only the VP23 dimer is shown. (J) Stereo pair of the two VP23 subunits, which have been extracted from the averaged triplex and aligned to a similar orientation. Three putative helices are modeled in each of the VP23 subunits. The upper helix is labeled with an asterisk to highlight its differing alignments in the two monomers.

eters and their subsequent projection-based refinement were carried out on a 24-processor SGI Onyx 2 supercomputer with procedures described previously (28), which are based on Fourier common lines [R. A. Crowther, *Philos. Trans. R. Soc. London Ser. B* **261**, 221 (1971); S. D. Fuller, *Cell* **48**, 923 (1987)]. Corrections for the contrast transfer function with an amplitude contrast of 10% [P. A. Thuman-Commike et al., *Biophys. J.* **76**, 2249 (1999)] and a Fourier amplitude decay factor of 180 Å² were performed for the reconstruction as described previously (15).

Viruses, W. Chiu, R. M. Burnett, R. L. Garcea, Eds. (Oxford Univ. Press, New York, 1997), pp. 312–351.

- B. Sodeik, M. W. Ebersold, A. Helenius, *J. Cell Biol.* **136**, 1007 (1997).
- W. Batterson, D. Furlong, B. Roizman, *J. Virol.* **45**, 397 (1983).
- W. W. Newcomb and J. C. Brown, *J. Virol.* **68**, 433 (1994).
- HSV-1 B capsids were purified by established procedures (22) and were quickly frozen in a thin layer of vitreous ice suspended across holes in a carbon-coated holey film. Flood beam illumination was used to record images on Kodak SO163 films. The first zero of the contrast transfer function of the first image is in the range of 1/17 to 1/6 Å⁻¹. The second image was taken at about 2 μ m farther away from the defocus of the first image. The second image, which was not included in the final reconstruction, was used to provide the orientation estimation for the corresponding particles in the first image. The micrographs were digitized with a Zeiss SCAI microdensitometer (Carl Zeiss, Englewood, CO) with a 7- μ m step size (corresponding to 1.4 Å per pixel on the specimen).
- Determination of the center and orientation param-

- eters and their subsequent projection-based refinement were carried out on a 24-processor SGI Onyx 2 supercomputer with procedures described previously (28), which are based on Fourier common lines [R. A. Crowther, *Philos. Trans. R. Soc. London Ser. B* **261**, 221 (1971); S. D. Fuller, *Cell* **48**, 923 (1987)]. Corrections for the contrast transfer function with an amplitude contrast of 10% [P. A. Thuman-Commike et al., *Biophys. J.* **76**, 2249 (1999)] and a Fourier amplitude decay factor of 180 Å² were performed for the reconstruction as described previously (15).
- Z. H. Zhou et al., *Nature Struct. Biol.* **2**, 1026 (1995).
- B. Böttcher, S. A. Wynne, R. A. Crowther, *Nature* **386**, 88 (1997).
- J. F. Conway et al., *Nature* **386**, 91 (1997).
- B. L. Trus et al., *Nature Struct. Biol.* **4**, 411 (1997).
- P. T. Wingfield et al., *J. Virol.* **71**, 8955 (1997).
- F. J. Rixon, unpublished data.
- Z. H. Zhou, D. H. Chen, J. Jakana, F. J. Rixon, W. Chiu, *J. Virol.* **73**, 3210 (1999).
- Z. H. Zhou et al., *Proc. Natl. Acad. Sci. U.S.A.* **95**, 2778 (1998).
- P. Desai and S. Person, *Virology* **261**, 357 (1999).
- R. C. Liddington et al., *Nature* **354**, 278 (1991).

- J. M. Grimes et al., *Nature* **395**, 470 (1998).
- B. L. Trus et al., *J. Mol. Biol.* **263**, 447 (1996).
- W. W. Newcomb et al., *J. Mol. Biol.* **232**, 499 (1993).
- Z. H. Zhou, B. V. Prasad, J. Jakana, F. J. Rixon, W. Chiu, *J. Mol. Biol.* **242**, 456 (1994).
- A. Saad, Z. H. Zhou, J. Jakana, W. Chiu, F. J. Rixon, *J. Virol.* **73**, 6821 (1999).
- Z. H. Zhou et al., data not shown.
- M. D. Kirkitadze et al., *J. Virol.* **72**, 10066 (1998).
- M. G. Rossmann and J. E. Johnson, *Annu. Rev. Biochem.* **58**, 533 (1989); S. Harrison, D. C. Wiley, J. J. Skehel, in *Fields Virology*, B. N. Fields et al., Eds. (Lippincott-Raven, Philadelphia, 1996), vol. 1, pp. 59–100.
- S. A. Wynne, R. A. Crowther, A. G. Leslie, *Mol. Cell.* **3**, 771 (1999).
- Z. H. Zhou et al., *Biophys. J.* **74**, 576 (1998).
- Z. H. Zhou et al., *J. Struct. Biol.* **116**, 216 (1996).
- Supported by NIH, National Center for Research Resources, NSF, and the Human Frontier Science Program. Z.H.Z. is a Pew Scholar in Biomedical Sciences and a Basil O'Connor Starter Scholar of the March of Dimes Birth Defects Foundation. We thank M. F. Schmid for discussions.

4 January 2000; accepted 29 February 2000